Supplementary Materials for

The intestinal microbiota programs diurnal rhythms in host metabolism through histone deacetylase 3

Zheng Kuang, Yuhao Wang, Yun Li, Cunqi Ye
Kelly A. Ruhn, Cassie L. Behrendt, Eric N. Olson, Lora V. Hooper

correspondence to: Lora.Hooper@UTSouthwestern.edu

This PDF file includes:

Materials and Methods
Figures S1 to S11
Tables S1, S3-S5

Other Supplementary Materials for this manuscript includes the following:

Table S2

Materials and Methods

Mice

Wild-type C57BL/6, *Hdac3*$^{fl/fl}$ (*28*), *Hdac3*$^{\Delta IEC}$, *Nr1d1*$^{-/-}$ (REV-ERBα-deficient) and *Myd88*$^{-/-}$ mice were bred and maintained in the SPF barrier at the University of Texas Southwestern Medical Center. *Hdac3*$^{fl/fl}$ mice (*28*) were used to generate intestinal epithelial cell (IEC)-specific *Hdac3* knockout mice (*Hdac3*$^{\Delta IEC}$) by crossing with a mouse expressing Cre recombinase under the control of the IEC-specific *Villin* promoter (*29*). Germ-free (GF) C57BL/6 mice were bred and maintained in the gnotobiotic mouse facility at the University of Texas Southwestern Medical Center as described (*30*). All mice were housed under a 12-hour light and 12-hour dark cycle unless otherwise specified. Mice were fed *ad libitum*. All experiments were performed using protocols approved by the Institutional Animal Care and Use Committee of the UT Southwestern Medical Center.

Jet lag experiments

Eight-week old *Hdac3*$^{fl/fl}$ and *Hdac3*$^{\Delta IEC}$ mice were housed in ventilated, light-tight cabinets on a 12-hour light and 12-hour dark cycle (Phenome Technologies). After acclimation for 3 days, light cycles were changed for mice subjected to experimental jet lag while the light cycles of control groups were left unchanged. Every 3 days, lights were turned on 8 hours earlier than the previous setting while maintaining a 24-hour light/dark cycle thereafter.

Diet

Mice were fed a regular chow diet (LabDiet 5KA1) containing 22% protein, 16% fat and 62% carbohydrates, or a Western style high fat diet (HFD) (TestDiet AIN-76A) containing 16% protein, 40% fat and 44% carbohydrates.

Metabolic studies

Mice were fed the HFD for 10 weeks before metabolic analysis. Antibiotic-treated mice were given an antibiotic cocktail containing 1 g/L streptomycin, 1 g/L gentamycin, 1 g/L neomycin, 1 g/L metronidazole and 0.5 g/L vancomycin throughout the HFD treatment. Body composition was measured with an EchoMRI^{TM}-100H analyzer. Blood glucose was measured using a One Touch Ultra2 glucose meter. Serum triglycerides were quantified using Infinity Triglycerides Liquid Stable Reagent (Thermo Scientific TR22421). Free fatty acids were measured using the Wako NEFA-HR(2) reagent (Wako 434-91795, 436-91995, 270-77000). Circadian oscillations of serum triglycerides were measured in mice fed *ad libitum* on a chow diet. Steady-state serum triglycerides, free fatty acids, and glucose tolerance were measured after an overnight fast. The insulin tolerance test was performed after a 4-hour fast. Mice were injected intraperitoneally with 2 mg/g body weight of D-(+)-glucose (Sigma G8769), or 0.5 U/kg body weight insulin (Eli Lilly, Humulin R) and blood glucose was measured at time 0, 15, 30, 60 and 100 minutes after injection. Real-time metabolic cage analysis was performed with the TSE Labmaster System.

Oil Red O detection of cellular lipids

Small intestines from *Hdac3*$^{fl/fl}$ and *Hdac3*$^{\Delta IEC}$ mice fed a HFD were rinsed with PBS and fixed in 10% formalin at room temperature for 2 hours. Tissues were rinsed with 2% sucrose in PBS and snap frozen in optimum cutting temperature (OCT) compound (Fisher 23-730.571). 7 μm sections were cut and mounted to Superfrost Plus Micro Slides (VWR). Oil Red O stock solution

(0.5 g/100 mL dissolved in isopropanol) was diluted with distilled water (6:4, V/V) and filtered through a 0.2 μm filter to make the working Oil Red O solution. Tissue sections were post-fixed with 10% formalin for 15 min, dipped in 60% isopropanol, and stained with the Oil Red O working solution for 30 min. Slides were then destained in 60% isopropanol and rinsed under running tap for 2 min. Images were captured using a Zeiss AxioImager M1 microscope.

Lipid quantification in intestinal epithelial cells

Ileal IECs from *Hdac3*$^{fl/fl}$ and *Hdac3*$^{\Delta IEC}$ mice on HFD were isolated using 10 mM EDTA as previously described (*7*). 10-20 mg IECs from each sample were used for lipid extraction using the Lipid Extraction Kit (Cell Biolabs STA-162). Extracted lipids were air dried, resuspended in 100 μl cyclohexane, and quantified using a Lipid Quantification Kit (Cell Biolabs STA-613). Lipid concentrations were normalized to cell weight.

Neutral lipid quantification in fecal pellets

Fresh fecal pellets from *Hdac3*$^{fl/fl}$ and *Hdac3*$^{\Delta IEC}$ mice fed the HFD were collected and weighed. Fecal lipids were extracted using a Lipid Extraction Kit (Cell Biolabs STA-612). Extracted lipids were air dried, resuspended in 100 μl isopropanol, and quantified using a Lipid Quantification Kit for neutral lipids (Cell Biolabs STA-617). Concentrations were normalized to feces weight.

Liquid chromatography (LC) with mass spectrometry (MS) analysis

Freshly prepared serum was quenched immediately with the same volume of chilled (-20°C) HPLC-grade methanol and spun for 20 min at 16,000 RCF in a tabletop centrifuge. The supernatants were collected and dried in a vacuum concentrator. Extracted metabolites were resuspended in detection buffers, separated chromatographically on a C_{18} column, and detected using an AB SCIEX 3200 QTRAP triple quadrupole mass spectrometer with different targeted LC-MS/MS methods as previously described (*31, 32*).

Laser capture microdissection and RNA purification

Laser capture microdissection was performed as previously described (*33*). Briefly, a 5 cm length of mouse ileum was washed and snap-frozen in OCT compound (Fisher 23-730.571). 7 μm frozen sections were cut and fixed in 70% ethanol and sequentially stained with Methyl Green and eosin. Laser capture microdissection of IECs was performed using an Arcturus PixCell IIe system. 5000-10000 cells were obtained from each section in one hour, and RNA was immediately extracted from the captured IECs by incubating with 14 μl RNA extraction buffer from the PicoPure RNA Isolation Kit (Life Technology 12204-01) for 30 min. Extracted RNA was purified using PicoPure RNA Isolation Kit.

Quantitative real-time PCR (RT-qPCR)

cDNA was synthesized from purified RNA using M-MLV Reverse Transcriptase (Fisher 28025021), qRT-PCR was performed using Platinum SYBR Green RT-qPCR SuperMix (Fisher 11733046) on a QuantStudio 7 Flex Real-Time PCR System (Applied Biosystems). Expression levels were calculated relative to the abundance of *Gapdh* transcripts. Primer sequences are listed in Table S1.

Chromatin immunoprecipitation (ChIP)

Mouse ileum tissues were washed with ice-cold PBS and IECs were extracted in 10 mM EDTA. The ChIP assay was carried out as previously described (*34, 35*) with a few modifications. Briefly, cells were washed with ice-cold PBS twice and fixed in 1% formaldehyde at room temperature for 10 min. Cells were then quenched in 125 mM glycine for 10 min, washed twice with PBS, resuspended in 0.5 ml lysis buffer (20 mM Tris-HCl, pH 8, 60 mM KCl, 1 mM EDTA, 0.5% NP-40 with protease inhibitors), and incubated at 4^{o}C for 15 min. Nuclei were pelleted and resuspended in 250 µl RIPA buffer (Thermo Scientific 89900) with protease inhibitors and sonicated with a Bioruptor Pico sonication device (Diagenode) for 20 cycles (30 sec on, 30 sec off). The supernatant was pre-cleared with 10 µl protein G magnetic beads for 1 h and then incubated with 3 µg of primary antibodies overnight at 4^{o}C. The antibodies used were: anti-H3K9ac (Abcam ab4441), anti-H3K27ac (Abcam ab4729), anti-HDAC3 (Abcam ab7030), anti-PGC-1α (Millipore, ST1204), anti-ERRα (Millipore 17-603). 50 µl protein G beads were added and incubated for 1.5 h at 4^{o}C. Beads were washed four times with LiCl wash buffer (100 mM Tris-HCl pH 7.5, 500 mM LiCl, 0.5% NP-40, 0.5% sodium deoxycholate) and finally with TE buffer. DNA was eluted in 150 µl TES buffer (TE with 1% SDS, 150 mM NaCl, and 5 mM dithiothreitol) by resuspending the beads at 65^{o}C for 8 h. DNA was purified using ChIP DNA Clean & Concentrator (Zymo Research D5205). ChIP DNA was either used for sequencing or quantitative PCR (qPCR). For ChIP-qPCR, relative enrichment was calculated by first normalizing all the signals from immunoprecipitated DNA to the signals from input DNA and further normalizing signals from binding regions to control regions. Binding region refers to known binding sites for each mark at the gene of interest and control region refers to the neighboring regions that lack binding sites.

Western blot

Mouse ileum tissues were washed with ice-cold PBS and IECs were isolated in 10 mM EDTA as previously described (*7*). Cells were washed twice with PBS and resuspended in 250 µl RIPA buffer (Thermo Scientific 89900) with protease inhibitors and sonicated with a Bioruptor Pico sonication device (Diagenode) for 10 cycles (30 sec on, 30 sec off). Supernatant protein concentrations were measured using the Pierce BCA Protein Assay Kit (Thermo 23225) and normalized across samples. Lysates were separated on 4-20% gradient SDS-PAGE gels and transferred to PVDF membranes. Membranes were blocked with 5% nonfat milk in TBS-T buffer (0.1% Tween-20 in Tris-buffered saline) for 1 h at room temperature then sequentially incubated with primary antibodies: anti-CD36 (ThermoFisher PA1-16813), anti-actin (Sigma, A5060), anti-Lamin B (abcam ab133741), anti-PGC-1α (Millipore, ST1202), anti-HDAC3 (Abcam ab7030), and appropriate HRP-conjugated secondary antibodies. Protein bands were visualized using a Bio-Rad ChemiDoc system.

Co-immunoprecipitation

Mouse ileum tissues were washed with ice-cold PBS and IECs were isolated in 10 mM EDTA as previously described (*7*). Cells were washed twice with PBS and resuspended in NP40 IP lysis buffer (20 mM Tris-HCl, pH 8.0, 150 mM NaCl, 10% glycerol, 2 mM EDTA, 0.1% NP40, 10 mM NaF, 1 mM DTT, 2 mM phenylmethylsulfonylfluoride and protease inhibitors). Lysates were sonicated for 10 cycles (30 sec on, 30 sec off) and supernatants were pre-cleared with protein G beads. After normalizing protein concentration, 3 µg of primary antibodies (anti-PGC-1α (Millipore, ST1204); anti-HDAC3 (Abcam ab7030); anti-rabbit IgG (ThermoFisher 02-

6102)) were added and incubated at 4°C for 2 hours. Next, protein G magnetic beads were added and incubated at 4°C for 1 hour. Beads were washed with NP40 IP lysis buffer four times and samples were eluted in 2X SDS loading buffer at 95°C for 5 min. Eluted proteins were separated on a 4-20% gradient SDS-PAGE gel and transferred to a PVDF membrane. The membrane was incubated with primary antibodies overnight and detected using a Bio-Rad ChemiDoc system. Input proteins were detected with anti-HDAC3 (Abcam, ab187945), anti-PGC-1α (Millipore, ST1202), anti-NCoR1 (Abcam, ab3482), and anti-actin antibody (Sigma, A5060).

Immunostaining

Mouse ileum tissues were washed with PBS, fixed in Bouin's fixative overnight at 4°C and embedded in paraffin. Sections were washed in xylene twice and rehydrated in decreasing concentrations of ethanol (100%, 95%, 70%, 50%, 0%). Slides were boiled in 10 mM sodium citrate for 15 min and washed in PBS twice. Slides were blocked with 10% FBS, 1% BSA, 1% Trixon X-100 in PBS for 1 hour and incubated with primary antibody (anti-HDAC3, ab7030, 1:200 dilution) at 4°C overnight. Cy3 anti-rabbit secondary antibody (Fisher 711-165-152) was diluted 1:400 and applied to slides for 1 hour at room temperature in the dark. Slides were washed and mounted with DAPI Fluoromount-G (Southern Biotechnology 0100-20). Images were captured using a Zeiss AxioImage MI microscope.

Conventionalization and monoassociation of germ-free mice

For conventionalization, ~50 mg feces were collected from a conventional wild-type mouse and suspended in 1 ml PBS. Fecal debris was pelleted and 200 µl of the supernatant was used for oral gavage of each GF mouse. Mice were sacrificed 1, 3 and 7 days after colonization. For monoassociations, GF mice were colonized with 2 x 10^9 colony forming units (cfu) of log phase *Bacteroides thetaiotaomicron* (VPI-5482), *Enterococcus faecalis* (ATCC-29212), *Escherichia coli* K235 (ATCC-13027) or *E. coli* O127:K63 (ATCC-12740), or with 1 x 10^9 cfu of log phase *Salmonella typhimurium* (strain 1433) through oral gavage. Mice were sacrificed 3 days after colonization.

Luciferase assay

A 1296 bp fragment of *Cd36* promoter (variant 5, NM_001159556.1) was fused to a firefly luciferase reporter (pGL3 promoter vector). ~1.5 kb fragments of *Cd36* enhancers were fused to pGL4.24 enhancer luciferase vector. 2 x 10^4 MODE-K cells were seeded into each well of a 96-well plate one day before transfection. 90 ng of empty vector, or protein expression vectors were transfected together with 30 ng *Cd36* reporter vector and 10 ng Renilla reporter vector. 24 hours after transfection, luciferase activities were determined using the Dual-Glo Luciferase Assay System (Promega E2920) following the manufacturer's protocol. The Renilla luciferase co-reporter was used to normalize luciferase activity.

RNA-seq and data analysis

RNA was extracted, pooled and purified from ileal epithelial cells of three mice at each time point across a 24-hour circadian cycle. RNA quality was examined by an Agilent 2100 Bioanalyzer. Libraries were prepared using a TruSeq RNA sample preparation kit v2 (Illumina) and sequencing was performed on Illumina NextSeq for single-end 75 bp length reads. Data were analyzed as previously described (*7*). Sequence data were mapped against the mm10 genome using TopHat (*36*) and FPKMs were generated using Cuffdiff (*36*) with default

parameters. Circadian oscillation was analyzed by ARSER (*37*). Details are provided below in the Circadian Analysis section. Absolute amplitudes were directly output by ARSER and relative amplitudes were calculated by dividing absolute amplitudes to the average expression levels. Expression levels of genes with circadian adjusted *P* Values < 0.05 (by ARSER) or $\log_2$ fold changes of circadian amplitudes > 1 or $\log_2$ fold changes of FPKMs > 1 or < -1 were plotted in heat maps. Gene Ontology analysis was performed using the online tool DAVID Bioinformatics Resources (https://david.ncifcrf.gov/).

ChIP-seq and data analysis

ChIP-seq libraries were generated using a KAPA Hyper Prep Kit (kapabiosystems KK8502) and library sizes and concentrations were evaluated by Bioanalyzer and RT-qPCR. Sequencing was performed on Illumina HiSeq 2500 or 4000 for single-end 50 bp length reads. Data analysis was as previously described (*34, 38*). Sequence data were mapped against the mm10 genome using BowTie2 (*39*) and signals were normalized by the total numbers of aligned reads and visualized by the UCSC Genome Browser. Peaks were detected by MACS (*40*) with a cutoff of peak length >100 and $-\log_{10}$ (P values) > 50. Peaks of the same mark were merged across CV and/or GF samples from all time points. Spatial analysis between different peaks and genomic features were performed using "countOverlaps" function in R. Circadian analysis was performed by first counting read intensities at peaks. Circadian characteristics were further calculated using ARSER. Heat maps were generated by first counting reads across consecutive 50 bp bins across each peak and plotting the values using "heatmap.2" function in R. DNase sensitivity (GSE57919), HDAC3 and ERRα ChIP-seq (GSE63964) data were downloaded from GEO and analyzed as described above.

Circadian analysis

Circadian analysis included a combination of statistical methods to 1) determine if an oscillation is statistically significant; and 2) determine if the amplitudes of two rhythms are significantly different.

a) We used ARSER, a circadian analysis program to determine whether histone acetylation, gene expression, or metabolite production was rhythmic when sampling at least 4 time points.
b) We used Fisher's Exact Test to evaluate rhythms when a sample was examined at 2 time points.
c) Amplitudes of oscillations in metabolite concentrations were first calculated for each replicate. Student's *t*-test was then used to determine whether the amplitudes of two rhythms were significantly different or not.
d) Amplitudes of histone acetylation ChIP-seq data and RNA-seq data were evaluated with a combination of Fisher's Exact Test and the permutation test. The maximum and minimum values of a rhythm were identified and used for Fisher's Exact Test. For the permutation test, we first calculated the ratio of amplitudes from two rhythms as the test statistic, T_{obs}. Next we randomly sampled values from the two original rhythmic sets with replacement and recalculated the amplitude ratio for every possible permutation. The one-sided P value was calculated as the proportion of sampled permutations where the amplitude ratio is less than or equal to T_{obs}.

e) All P values were either automatically adjusted for multiple comparisons by ARSER, or adjusted to FDR using p.adjust() function in R.

Using a combination of these approaches, we were able to first identify whether a target was rhythmic under one condition but not rhythmic under another condition when adjusted $P_1 < 0.05$ and adjusted $P_2 > 0.05$. When both rhythms were significant, we could determine if the oscillation was dampened by testing if the amplitude was changed.

16*S* rRNA sequencing and data analysis

Fecal DNA was purified from freshly collected feces using the FastDNA Spin Kit (MP Biomedicals 116560-200) and a FastPrep-24 5G Homogenizer. Sequencing libraries were prepared using the HotStarTaq Plus Master Mix Kit (Qiagen) with primers flanking variable regions V3-V4. Sequencing was performed on a MiSeq following the manufacturer's guidelines. Operational taxonomic units (OTUs) were defined by clustering at 3% divergence (97% similarity). Final OTUs were taxonomically classified using BLASTn against a curated database derived from RDPII and NCBI. Principle component analysis was performed using the "prcomp" function in R and differential abundance analysis was performed using DESeq2 (*41*).

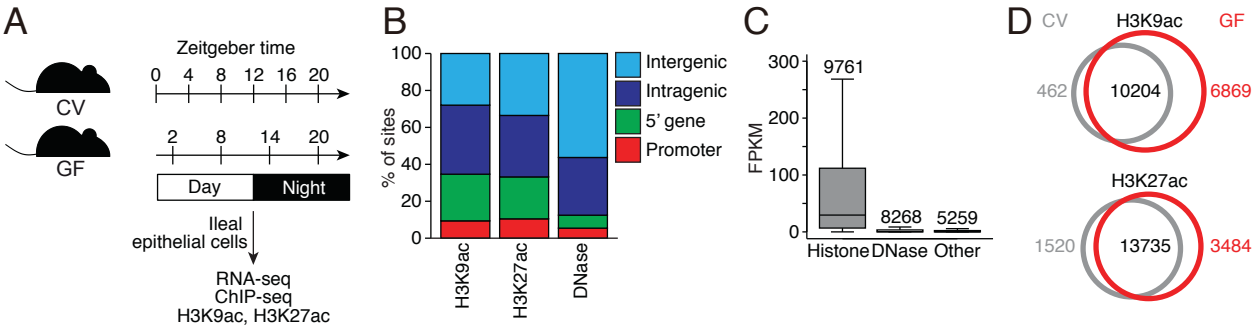

Figure S1. Chromatin analysis of intestinal epithelial cells from conventional and germ-free mice. (**A**) Strategy for chromatin landscape characterization and gene expression analysis. (**B**) Percentages of marks located at promoters, the 5' end of genes, intragenic and intergenic regions. (**C**) Expression levels of transcripts associated with both histone and DNase marks (Histone), DNase mark only (DNase) and neither histone nor DNase marks (Other). (**D**) Venn diagrams showing the spatial similarity of histone acetylation peaks in intestinal epithelial cells from CV and GF mice. Numbers of unique and common peaks between CV and GF samples are indicated. CV, conventional; GF, germ-free; FPKM, Fragments Per Kilobase of transcript per Million mapped reads.

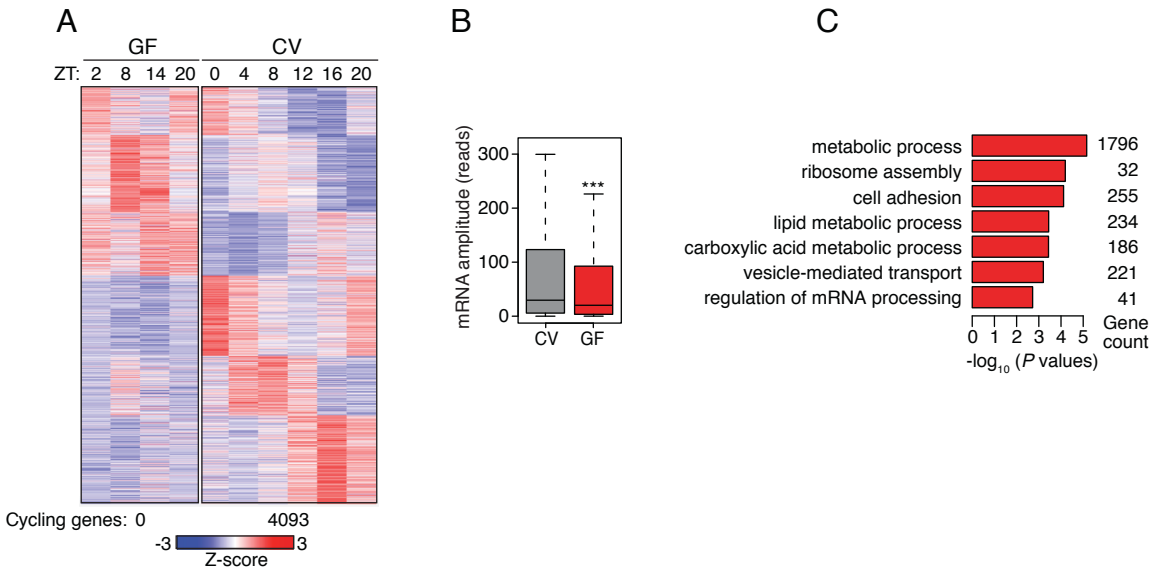

Figure S2. Transcriptome analysis of intestinal epithelial cells from conventional and germ-free mice. (**A**) Heat map shows the expression pattern for cycling transcripts across a 24-hour cycle in GF and CV (*7*) epithelial cells (3 pooled biological replicates per library). Rhythmicity was calculated by ARSER and the numbers of cycling transcripts are shown at the bottom of the heat map ($P < 0.05$). (**B**) Amplitudes of oscillating transcripts from CV and GF mice. ***, P<0.001. (**C**) Enriched Gene Ontology categories among cycling transcripts. CV, conventional; GF, germ-free; ZT, Zeitgeber time.

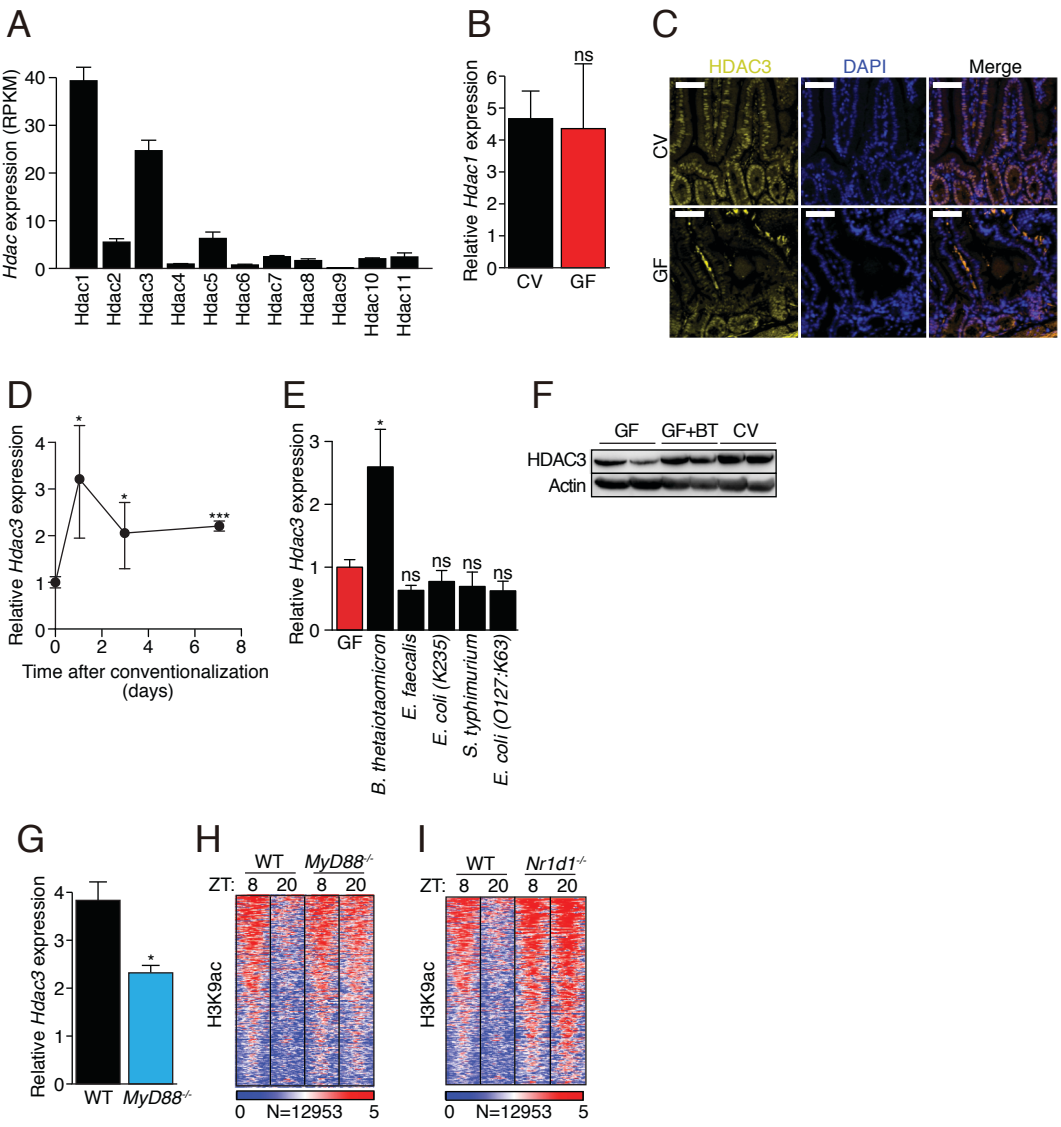

Figure S3. Analysis of *Hdac* expression in intestinal epithelial cells. (**A**) Expression of *Hdac* transcripts in IECs from conventional mice was assessed by RNA-seq (*7*). (**B**) qRT-PCR analysis of *Hdac1* transcript abundances in CV and GF mice. (**C**) Immunofluorescence detection of HDAC3 in mouse small intestine. Scale bars=50 μm. (**D**) qRT-PCR analysis of *Hdac3* transcript abundance in IECs from GF mice following conventionalization. N=3 mice per group. (**E**) qRT-PCR analysis of *Hdac3* transcript abundance in IECs from GF mice following monocolonization with *Bacteroides thetaiotaomicron*, *Enterococcus faecalis*, *Salmonella typhimurium*, the non-pathogenic *Escherichia coli* strain K235 or the pathogenic *E. coli* strain O127:K63. N=3 mice per group. (**F**) Western blot of HDAC3 and actin (loading control) in IECs from CV and GF mice and GF mice after monocolonization with *Bacteroides thetaiotaomicron*. (**G**) qRT-PCR analysis of *Hdac3* expression in epithelial cells from WT and *Myd88*$^{-/-}$ mice. N=3 mice per group. (**H,I**) Heat map of H3K9ac signals (log (reads at 50 bp windows)) from -1 to +1 kb surrounding the centers of all cycling H3K9ac peaks in epithelial cells from WT and *Myd88*$^{-/-}$ mice (**H**) or *Nr1d1*$^{-/-}$ mice (**I**). N=3 mice per group; *, P<0.05; ***, P<0.001 by two-tailed *t*-test; ns, not significant. Means±SEM (error bars) are plotted. RPKM, reads per kilobase, per million mapped reads; CV, conventional; GF, germ-free; WT, wild-type; ZT, Zeitgeber time.

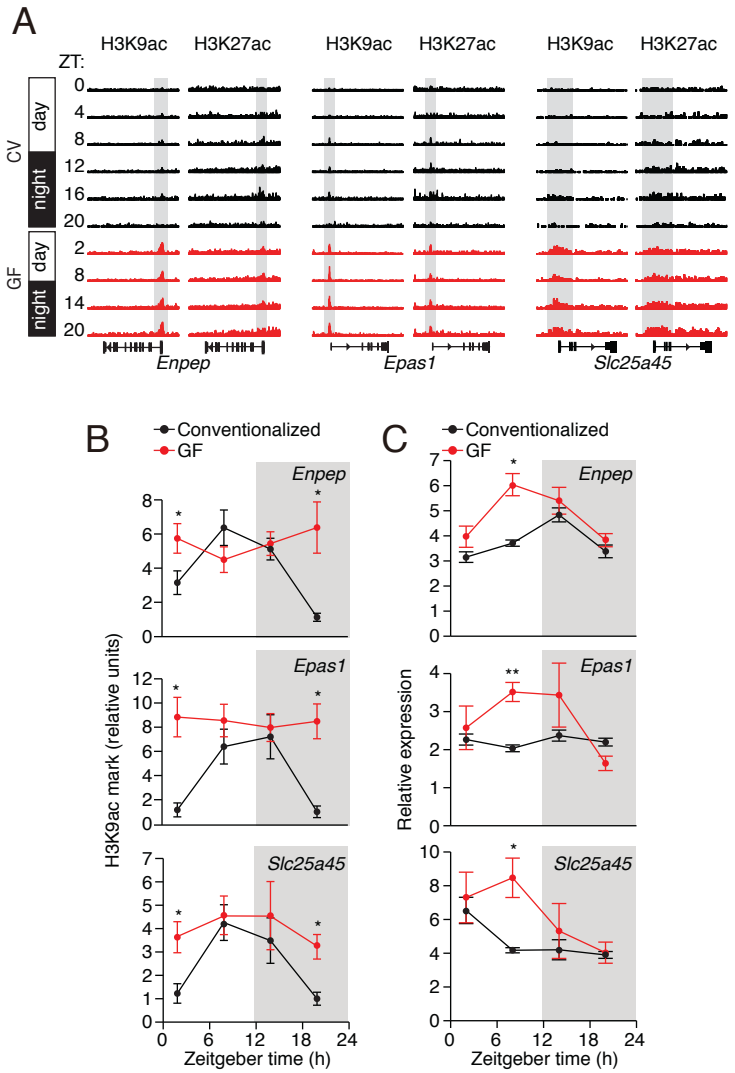

Figure S4. Histone acetylation at *Enpep*, *Epas1*, and *Slc25a45* in small intestinal epithelial cells exhibits diurnal rhythmicity that depends on the microbiota. (**A**) Genome browser view of each gene, showing ChIP-seq analysis of H3K9ac and H3K27ac marks (gray highlights) in IECs. The analysis was done across a circadian cycle in CV and GF mice. Each track represents the normalized ChIP-seq read coverage at a single time point. N=3 pooled biological replicates per library. (**B**) ChIP-qPCR of H3K9ac at each gene and (**C**) RT-qPCR of each transcript in small intestinal epithelial cells from GF mice and GF mice following conventionalization. N=3 mice per group; *, $P<0.05$; **, $P<0.01$ by two-tailed *t*-test; CV, conventional; GF, germ-free; ZT, Zeitgeber time.

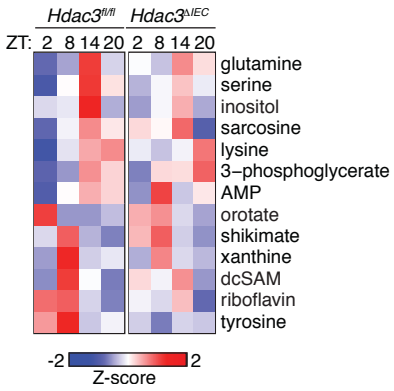

Figure S5. *Hdac3*$^{\Delta IEC}$ mice show altered diurnal rhythms in serum metabolites. Serum metabolites were quantified by liquid chromatography and tandem mass spectrometry across a 24-hour day-night cycle and the data are represented as a heat map. Each value in the heat map is the average of three measurements from 3 mice per group. ZT, Zeitgeber time.

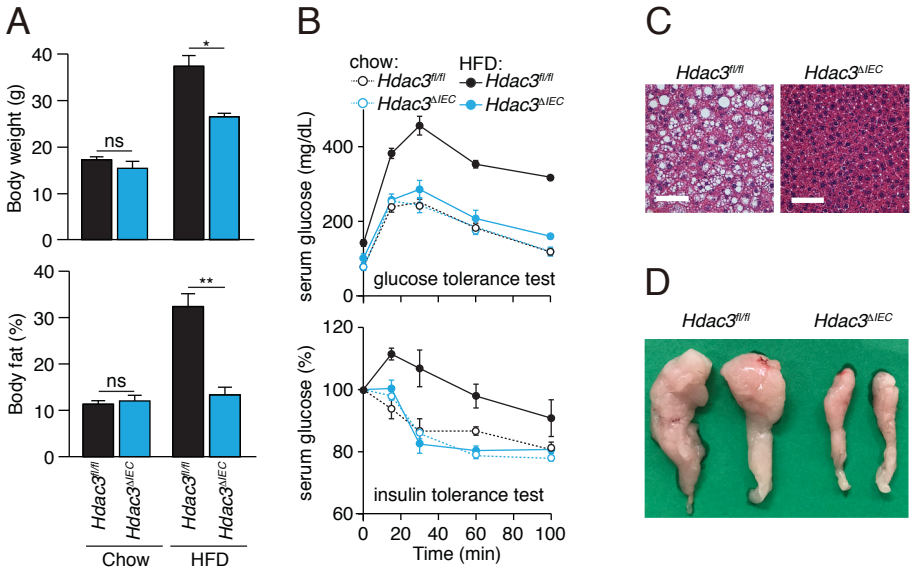

Figure S6. Metabolic phenotypes of *Hdac3*$^{fl/fl}$ and *Hdac3*$^{\Delta IEC}$ mice. (**A**) Weight and body fat percentages of *Hdac3*$^{fl/fl}$ and *Hdac3*$^{\Delta IEC}$ mice fed a chow diet or a high fat diet (HFD) for 10 weeks. N=5 mice per group. **P*<0.05; ***P*<0.01; ns, not significant by two-tailed *t*-test. Means±SEM (error bars) are plotted. (**B**) Glucose tolerance and insulin tolerance tests in *Hdac3*$^{fl/fl}$ and *Hdac3*$^{\Delta IEC}$ mice fed a chow or a HFD. N=3 mice per group. (**C**) Hematoxylin & eosin staining of liver from *Hdac3*$^{fl/fl}$ and *Hdac3*$^{\Delta IEC}$ mice fed a HFD for 10 weeks. Scale bars=100 μm. (**D**) Epididymal fat pads of *Hdac3*$^{fl/fl}$ and *Hdac3*$^{\Delta IEC}$ mice fed a HFD for 10 weeks. Pictures are representative of three replicates.

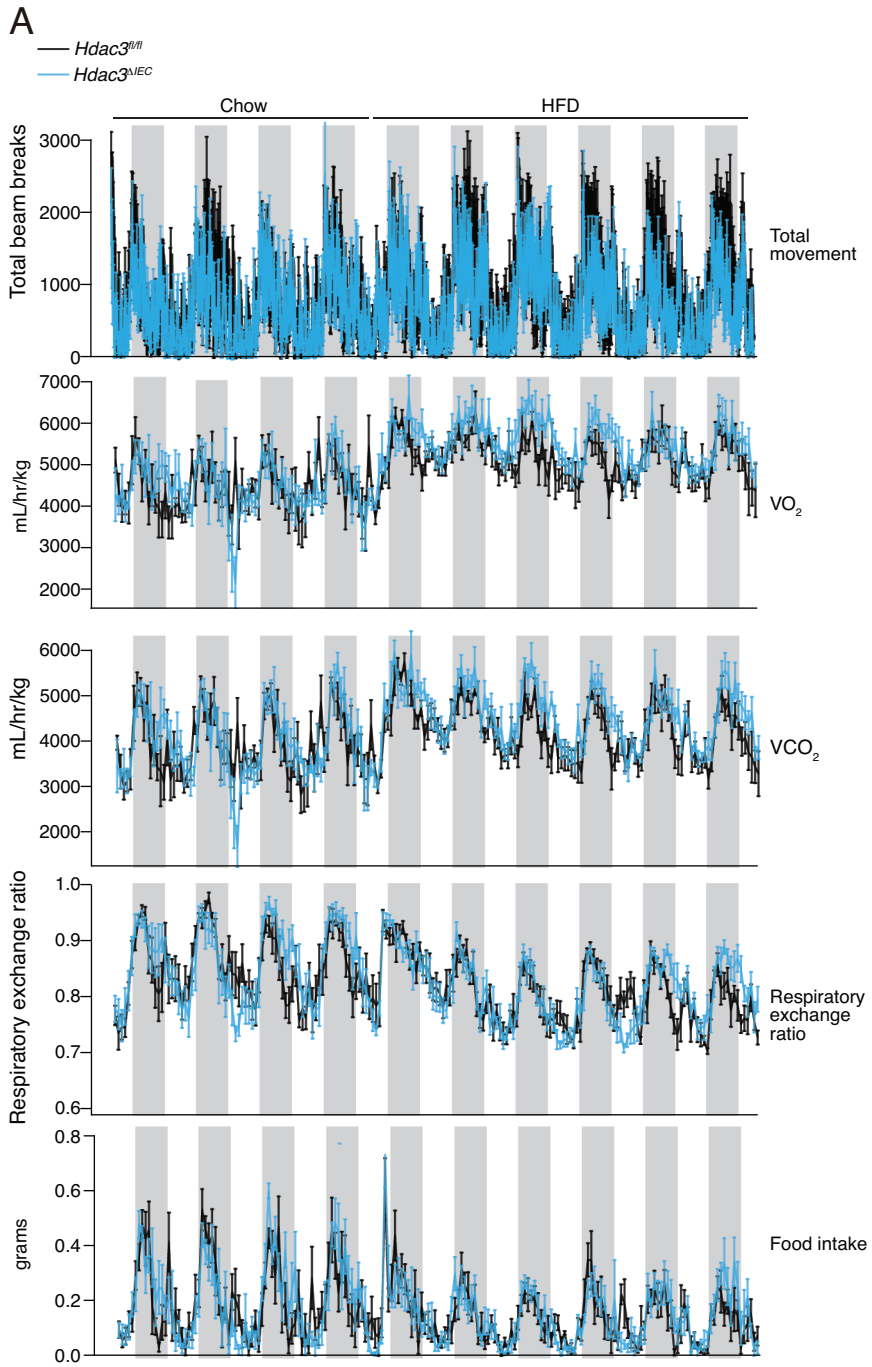

Figure S7. Physical activity, energy utilization and food uptake are similar in *Hdac3*$^{fl/fl}$ and *Hdac3*$^{\Delta IEC}$ mice. (**A**) Total movement, oxygen consumption rate, CO_2 production rate, respiratory exchange ratio and food intake of mice was recorded over 10 days. (**B**) Food intake of *Hdac3*$^{fl/fl}$ and *Hdac3*$^{\Delta IEC}$ mice during day and night. (**C**) Food intake of *Hdac3*$^{fl/fl}$ and *Hdac3*$^{\Delta IEC}$ mice fed a chow diet or high fat diet (HFD). All other mice were fed a chow diet during the first 4 days and a HFD over the following days. N=6 mice per group. ns, not significant by two-tailed *t*-test. Error bars represent SEM.

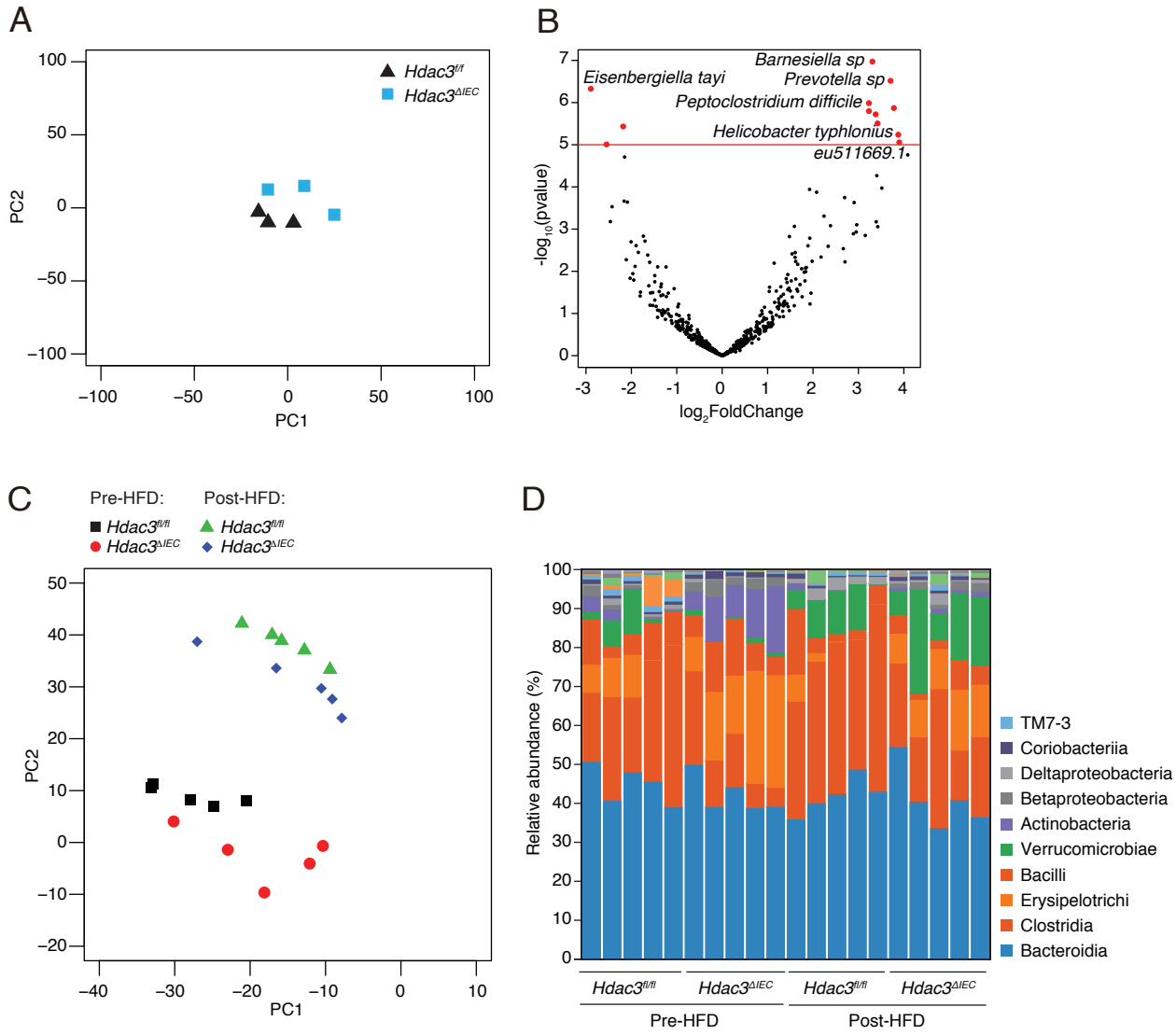

Figure S8. *Hdac3*$^{fl/fl}$ and *Hdac3*$^{\Delta IEC}$ mice share similar intestinal microbiotas. (**A**) Principal coordinate analysis of 16*S* rRNA sequencing of fecal samples from *Hdac3*$^{fl/fl}$ and *Hdac3*$^{\Delta IEC}$ mice. The mice were littermates of heterozygous crosses that remained cohoused. Each dot represents one mouse. (**B**) Volcano plot showing bacterial species with differential abundances in *Hdac3*$^{fl/fl}$ and *Hdac3*$^{\Delta IEC}$ mice. N=3 mice per group. (**C**) Principal coordinate analysis of 16*S* rRNA sequencing of fecal samples from *Hdac3*$^{fl/fl}$ and *Hdac3*$^{\Delta IEC}$ mice before or after HFD treatment. (**D**) Relative abundance of bacterial classes from *Hdac3*$^{fl/fl}$ and *Hdac3*$^{\Delta IEC}$ mice before or after HFD treatment. N=5 mice per group.

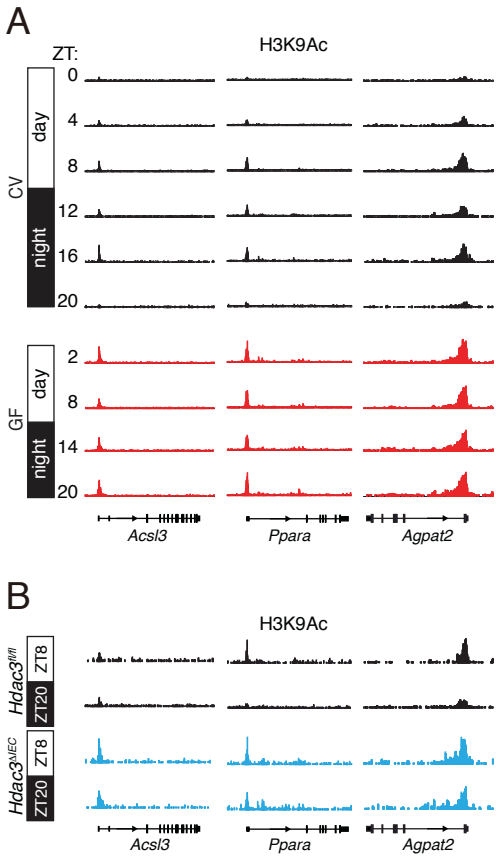

Figure S9. Histone acetylation at *Acsl3*, *Ppara*, and *Agpat2* in small intestinal epithelial cells exhibits diurnal rhythmicity that depends on the microbiota and *Hdac3*. Genome browser view of each gene showing ChIP-seq analysis of H3K9ac marks in small intestinal epithelial cells. The analysis was done across a circadian cycle in CV and germ-free GF mice (**A**), and at ZT8 and ZT20 in *Hdac3*$^{fl/fl}$ and *Hdac3*$^{\Delta IEC}$ mice (**B**). Each track represents the normalized ChIP-seq read coverage at a single time point. N=3 pooled biological replicates per library. CV, conventional; GF, germ-free; ZT, Zeitgeber time.

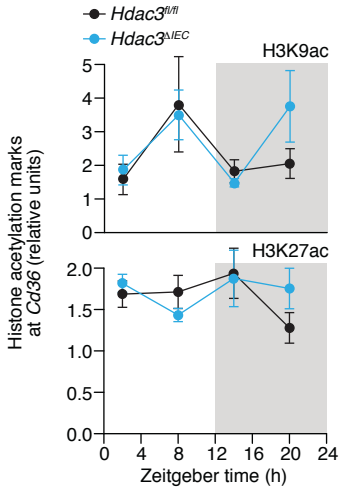

Figure S10. H3K9ac and H3K27ac marks at *Cd36* are not markedly altered in *Hdac3*$^{\Delta IEC}$ mice. ChIP-qPCR analysis of H3K9ac and H3K27ac marks at the *Cd36* promoter in IECs from *Hdac3*$^{fl/fl}$ and *Hdac3*$^{\Delta IEC}$ mice across a day-night cycle. N=3 mice per group.

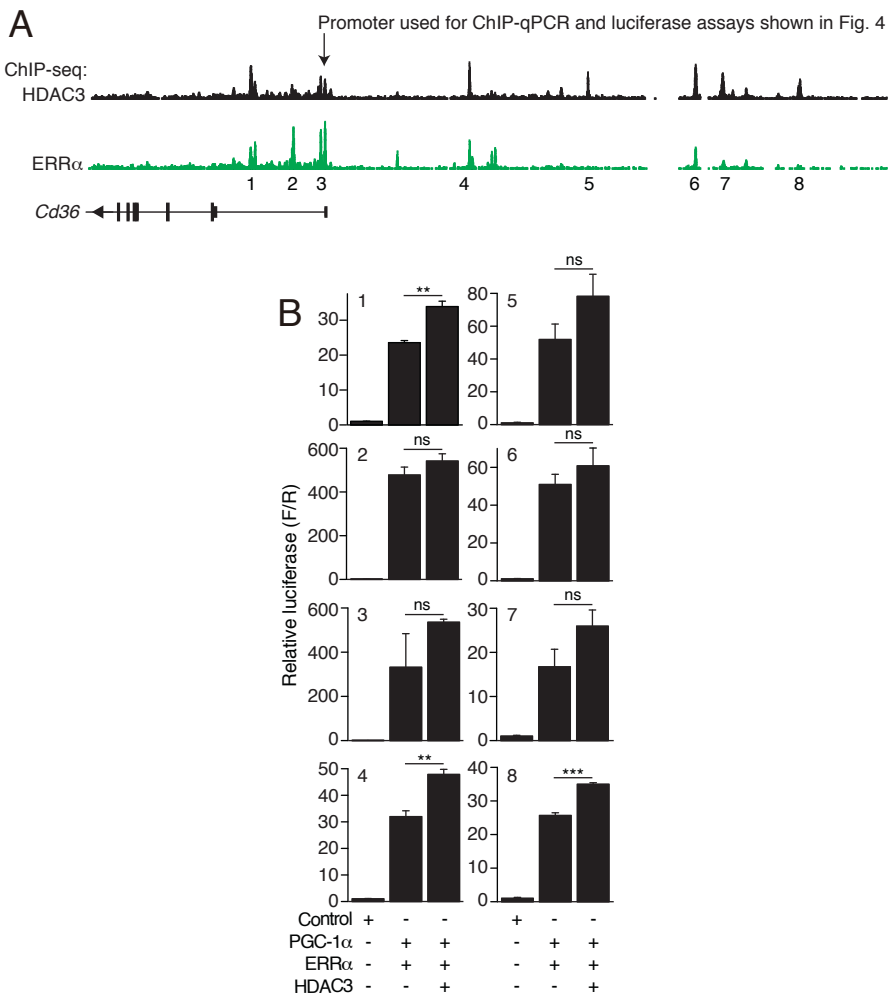

Figure S11. Transcriptional activation of *Cd36* by ERRα, PGC-1α and HDAC3. (**A**) Re-analysis of HDAC3 and ERRα ChIP-seq data collected from brown adipose tissue (*16*) shows that HDAC3 and ERRα colocalize at the *Cd36* promoter and enhancers. (**B**) Luciferase reporter assay of transcription driven by *Cd36* enhancers, demonstrating combinatorial effects of HDAC3, PGC-1α and ERRα. N=3 mice per group. $^{**}P$ <0.01; $^{***}P$<0.001; ns, not significant by two-tailed *t*-test; error bars represent SEM.

Table S1: Primer sequences

Primer	Sequence
Hdac3RTF	CACCAAGAGCCTTGATGCCTT
Hdac3RTR	GCAGCTCCAGGATACCAATTACT
Cd36RTF	TCATATTGTGCTTGCAAATCCAA
Cd36RTR	TGTAGATCGGCTTTACCAAAGATG
Cd36ChIPPosF	TCATCAAACAGCATGAATCTCC
Cd36ChIPPosR	TACCTGACAGATGGAAAGCAAA
Cd36ChIPCtrF	TCAGATGCTAATTTGTGGTTGG
Cd36ChIPCtrR	CCAGAAATAGACCCTTGTGAGC
Hdac1RTF	AGTCTGTTACTACTACGACGGG
Hdac1RTR	TGAGCAGCAAATTGTGAGTCAT
Slc25a45ChIPPosF	CCTAGCAGAGAGAGGCAGAGAC
Slc25a45ChIPPosR	GCCTGCCTACTACAGTTTTGCT
Slc25a45ChIPCtrF	TTACTTCTCAGGCCTCTTCCAG
Slc25a45ChIPCtrR	AACCCGATAACCTCCCACTAAT
EnpepChIPCtrF	GAAGCAAAGAGAAAAGGCAAAA
EnpepChIPCtrR	GGTGCTGAGCTGTATGTGCTAC
EnpepChIPPosF	TTGGCTCAGCGCTATATAAACA
EnpepChIPPosR	TTTGCCAAGTGATTTCTCTGAA
Epas1ChIPPosF	AAAGCAGAAATATTGGGACTCG
Epas1ChIPPosR	CAAGGAGTCTGTGTGAACTCCA
Epas1ChIPCtrF	AAAAGTGAGGCTGAAAGGACAC
Epas1ChIPCtrR	AACTGCGACTTGTTTTTGAGGT
EnpepRTF	TACATGGAGGACGGGCAAATC
EnpepRTR	GGTTCGTCGAAACAAGGGAAG
Epas1RTF	TCCTTCGGACACATAAGCTCC
Epas1RTR	GACAGAAAGATCATGTCACCGT
Slc25a45RTF	CCCTGGTCAACTCCGTCCT
Slc25a45RTR	TGGCTCTGTCTGGTTTTGTAGA
Universal_16S_F	AAACTCAAAKGAATTGACGG
Universal_16S_R	CTCACRRCACGAGTGAC

Table S2 is provided as a separate Excel file

Table S3: Statistical analysis of circadian rhythms of gene expression

CycID	WT circadian pvalue	Hdac3KO circadian pvalue	Amplitude P permutation	Amplitude P Fisher
Nr1d1	0.008935508	0.008377909	0.502	0.768572676
Nfil3	8.02E-05	0.001654271	0.511	0.614277036
Arntl	0.001485388	0.006605974	0.375	0.126535686
Per3	0.046743243	0.008720192	0.298	0.467808201
Per2	0.041434422	0.010418064	0.474	0.483581946
Slc7a6	0.037161542	0.059302552	0.188	0.474752728
Slc7a1	0.01499753	0.013952617	0.054	0.314173095
Slc38a2	0.000244027	0.186735262	0.238	0.194670131
Slc3a1	0.019587299	0.418913315	0.266	0.001378605
Slc6a14	0.025555738	0.013653479	0	1
Slc36a1	0.017784716	0.014833887	0.071	0.10758049
Slc16a10	0.001323093	0.005136318	0.023	0.334895473
Slc7a8	0.00082143	0.001939454	0.03	0.68354593
Slc5a11	0.000681423	0.000582257	0.017	0.799764243
Slc52a3	1.48E-05	0.218345107	0.03	2.24E-09
Slc6a19	0.040617788	0.003231368	0.13	2.26E-32
Slc7a9	0.004521603	0.292080606	0.283	2.82E-05
Slc7a7	0.000854425	7.85E-08	0.301	0.000918855
Slc3a2	8.70E-06	0.000286464	0.242	0.000846953
Mttp	0.01846664	0.020615187	0.046	0.538435484
Hadhb	0.000577601	0.073275378	0.418	0.271230611
Cftr	0.000993767	0.080124723	0.276	0.25762609
Apoc4	0.028527368	0.008588445	0.101	0.000975111
Slc27a2	0.063804038	0.075943554	0.129	0.029925704
Apoc3	0.097974041	0.024101399	0.241	1.15E-92
Apoc1	0.049532604	0.021898472	0.336	0.198603327
Apoc2	0.04552157	0.040482217	0.426	0.000122391
Apob	0.04138925	0.05717929	0.502	0.570545529
Acsl3	0.023290244	0.055137448	0.356	0.281843429
Cpt1a	9.99E-06	0.072082462	0.334	0.336944762
Cpt1b	0.011121872	0.323265492	0.146	0.17377316
Angptl4	0.039708299	0.012417569	0.162	2.40E-10
Agps	0.030143221	0.000237552	0.034	0.364635729
Scd1	0.044666091	0.131496481	0.03	1.06E-34
Scd2	0.004447726	0.889008048	0.108	2.00E-27
Ppara	7.05E-05	0.802583501	0.123	0.052269435
Agpat2	0.046441532	0.318297079	0.005	1.13E-33
Clps	0.046658685	0.195978817	0.003	0.375021041
Pla2g2a	0.027832948	0.351382877	0.026	0.639725642
Saa1	0.04122055	0.016796344	0.001	3.22E-07
Nr1h3	0.000254415	0.077707312	0.086	0.209430208
Agpat3	0.000116074	0.013830873	0.061	0.497425396
Fabp5	0.0002725	0.050152503	0.438	0.986912767
Ces1g	0.354457934	0.678276061	0.042	0.215177229
Cav1	0.013013115	0.007109913	0.016	0.24461851
Hsd11b1	0.04497323	0.146965782	0.356	0.687252307
Aqp7	0.048267612	0.000272966	0.043	0.055759093
Pparg	0.00601737	0.000752516	0.036	0.110975147
Cd36	0.027880477	0.008271377	0.014	0.05357201
Lpl	0.098508686	0.002583313	0.001	0.00202382
Cyp2e1	0.065982499	0.0058644	0.017	0.0026353
Thrsp	0.046344616	0.000379183	0.049	0.065017355
Fabp4	0.047783115	0.001795973	0.014	2.37E-13
Fasn	0.04977906	0.009434555	0.015	3.48E-05

Table S4: Statistical analysis of circadian rhythms of serum metabolites

Metabolites	WT circadian pvalue	Hdac3KO circadian pvalue
3-phosphoglycerate	0.011298701	0.294935065
AMP	0.041038961	0.119545455
dcSAM	0.005324675	1
glutamine	0.003798701	0.898636364
inositol	0.041038961	0.143598902
lysine	0.022272727	0.768149351
orotate	0.041038961	0.637662338
riboflavin	0.002272727	0.191233766
sarcosine	0.022272727	0.294935065
serine	0.003798701	0.538961039
shikimate	0.022272727	0.294935065
tyrosine	0.041038961	1
xanthine	0.041038961	0.129764087

Table S5: Statistical analysis of circadian rhythms of histone acetylation peaks at lipid metabolic genes

Gene marker	CV circadian pvalue	GF circadian pvalue	WT hdac3KO circadian pvalue
Ppara_H3K9ac	0.000427221	0.0796216	7.36E-46
Agpat2_H3K9ac	0.002247663	0.791842929	0.0001381
Acsl3_H3K9ac	0.001384638	0.208344273	0.04532114
Cpt1a_H3K9ac	0.000710092	0.503948127	0.0001232
Enpep_H3K9ac	0.000104928	0.062404161	
Epas1_H3K9ac	0.000480347	0.066711041	
Slc25a45_H3K9ac	0.00064621	0.389014215	
Enpep_H3K27ac	0.001702591	0.441075017	
Epas1_H3K27ac	0.004703911	0.290502174	
Slc25a45_H3K27ac	0.004323853	0.30019116	